Acta Crystallographica Section F
Structural Biology and Crystallization Communications
ISSN 1744-3091

The high-resolution structure of dihydrodipicolinate synthase from *Escherichia coli* bound to its first substrate, pyruvate

Sean R. A. Devenish,[a] Juliet A. Gerrard,[a] Geoffrey B. Jameson[b] and Renwick C. J. Dobson[c,d]*

[a]School of Biological Sciences, University of Canterbury, Private Bag 4800, Christchurch 8020, New Zealand, [b]Centre for Structural Biology, Institute of Fundamental Sciences, Massey University, Palmerston North 4474, New Zealand, [c]Department of Biochemistry and Molecular Biology, University of Melbourne, Parkville, Victoria 3010, Australia, and [d]Bio21 Molecular Science and Biotechnology Institute, 30 Flemington Road, University of Melbourne, Parkville, Victoria 3010, Australia

Correspondence e-mail: rdobson@unimelb.edu.au

Received 21 July 2008
Accepted 15 October 2008

PDB Reference: dihydrodipicolinate synthase, 3du0, r3du0sf.

Dihydrodipicolinate synthase (DHDPS) mediates the key first reaction common to the biosynthesis of (*S*)-lysine and *meso*-diaminopimelate, molecules which play a crucial cross-linking role in bacterial cell walls. An effective inhibitor of DHDPS would represent a useful antibacterial agent; despite extensive effort, a suitable inhibitor has yet to be found. In an attempt to examine the specificity of the active site of DHDPS, the enzyme was cocrystallized with the substrate analogue oxaloacetate. The resulting crystals diffracted to 2.0 Å resolution, but solution of the protein structure revealed that pyruvate was bound in the active site rather than oxaloacetic acid. Kinetic analysis confirmed that the decarboxylation of oxaloacetate was not catalysed by DHDPS and was instead a slow spontaneous chemical process.

1. Introduction

Dihydrodipicolinate synthase (DHDPS; EC 4.2.1.52) catalyses the first committed step in the biosynthesis of both (*S*)-lysine and *meso*-diaminopimelate: the condensation of pyruvate and (*S*)-aspartate-β-semialdehyde [(*S*)-ASA] to form (4*S*)-4-hydroxy-2,3,4,5-tetrahydro-(2*S*)-dipicolinic acid (HTPA; Fig. 1). The catalytic mechanism of DHDPS has been extensively studied and a number of crystal structures of DHDPS have been published (Blagova *et al.*, 2006; Blickling *et al.*, 1997, 1998; Dobson *et al.*, 2004, 2005; Kefala & Weiss, 2006; Pearce *et al.*, 2006; Kefala *et al.*, 2008). DHDPS is the second of two regulated enzymes in the biosynthesis of the aspartate family of amino acids, with the first being aspartate kinase (AK). Both DHDPS and AK are subject to feedback inhibition by (*S*)-lysine in some but not all species (Curien *et al.*, 2008). DHDPS is of interest as a potential target for genetic modification in crop plants owing to its role as the catalyst of the putative rate-limiting step in the biosynthesis of (*S*)-lysine, which is often a limiting nutrient (Miflin *et al.*, 1999; Frizzi *et al.*, 2008). DHDPS has also attracted attention as a potential target for antimicrobial drug and herbicide development as it is expressed in both microorganisms and plants but not in animals (Coulter *et al.*, 1999; Cox *et al.*, 2000; Hutton *et al.*, 2003). To date, no potent inhibitor has been found (Mitsakos *et al.*, 2008; Boughton *et al.*, 2008).

To investigate the active-site discrimination with a view to developing a set of structural parameters for future development of an effective active-site inhibitor, we carried out a cocrystallization of DHDPS with oxaloacetate. On solution of the X-ray crystal structure, we found that the enzyme clearly had pyruvate bound at both active sites in the asymmetric unit. The crystal structure presented here

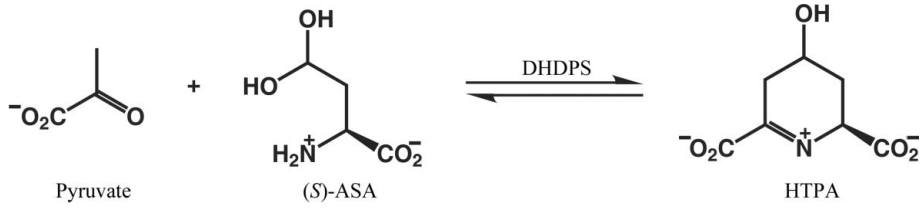

Figure 1
Reaction catalysed by DHDPS.

Table 1
Data-collection and refinement statistics.

Values in parentheses are for the highest resolution shell.

Resolution (data processing) (Å)	32.14–2.00 (2.05–2.00)
No. of images	272
Oscillation range (°)	0.25
Space group	$P3_121$
Unit-cell parameters (Å)	$a = b = 120.95$, $c = 110.03$
No. of reflections/unique reflections	256351/62822
Redundancy	4.08 (4.00)
Completeness (%)	99.6 (100.0)
R_{merge}†	0.083 (0.351)
Wilson B value (Å^2)	25.2
$I/\sigma(I)$	10.4 (3.7)
Resolution (refinement) (Å)	32.14–2.00 (2.05–2.00)
R_{free}‡	0.245 (0.385)
R_{cryst}§	0.188 (0.317)
Mean B values (Å^2)	
Protein	27.8
Water molecules	33.6
Estimated coordinate error¶ (Å)	0.12
Residues/water molecules	584/522
R.m.s.d.s from ideal geometry	
Bond lengths (Å)	0.010
Bond angles (°)	1.22

† $R_{merge} = \sum_{hkl}\sum_i |I_i(hkl) - \langle I(hkl)\rangle| / \sum_{hkl}\sum_i I_i(hkl)$. ‡ R_{free} is based on 5% of the total reflections excluded from refinement. § $R_{cryst} = \sum ||F_{obs}| - |F_{calc}|| / \sum |F_{obs}|$. ¶ Based on maximum-likelihood calculations.

provides data to a higher resolution than that previously reported (Blickling *et al.*, 1997; not deposited in the PDB) and has been deposited in the PDB (PDB code 3du0).

2. Methods and materials

2.1. Expression, purification and crystallization of DHDPS

DHDPS was expressed from an *Escherichia coli* XL-1 Blue cell line harbouring the plasmid pJG001 as previously described (Dobson *et al.*, 2005).

The crystallization experiments were undertaken as previously described (Dobson *et al.*, 2005) using the hanging-drop vapour-diffusion method at 277 K. Each drop contained 3 µl protein solution (~8 mg ml^{-1} in 20 m*M* Tris–HCl containing 100 m*M* oxaloacetate pH 8), 1.2 µl precipitant (1.8 *M* K_2HPO_4 pH 10) and 0.6 µl *N*-octyl-β-(*R*)-glucopyranoside [6%(*w*/*v*)]. Crystals appeared after 3–4 d and grew to dimensions of up to 0.3 mm. Before X-ray data collection, the crystals were soaked in cryoprotectant solution [1.8 *M* K_2HPO_4 pH 10 containing 100 m*M* oxaloacetate and 20%(*v*/*v*) glycerol] and directly flash-frozen in liquid nitrogen.

2.2. Data collection and processing

Intensity data were collected at 110 K using an R-AXIS IV^{++} image-plate detector coupled to a Rigaku Micromax 007 X-ray generator operating at 40 kV and 20 mA. The crystal belonged to space group $P3_121$ and diffracted to 2.0 Å resolution. The diffraction data set was processed and scaled using the program *CrystalClear* (Pflugrath, 1999). The merging R value was 0.083 (Table 1). The unit-cell parameters, Matthews coefficient (3.29 Å^3 Da^{-1}) and solvent content (62.3%) were consistent with those previously published (Mirwaldt *et al.*, 1995; Dobson *et al.*, 2004; Blickling *et al.*, 1997). The R_{free} set was transferred from the wild-type structure 1yxc (Dobson *et al.*, 2005) using the program *CAD* from the *CCP*4 suite (Collaborative Computational Project, Number 4, 1994).

2.3. Structure determination and refinement

Molecular replacement was carried out using the program *MOLREP* (Vagin & Teplyakov, 1997), using *E. coli* DHDPS (PDB code 1yxc, stripped of all nonprotein molecules) as a search model. The active-site lysine residue (Lys161) was initially modelled as an unmodified lysine residue until the electron density of the attached adduct was sufficiently clear to allow identification (see supplementary material[1]). Refinement was achieved using *REFMAC*5 (Vagin *et al.*, 2004) with manual model corrections using the program *Coot* (Emsley & Cowtan, 2004). The final refinement rounds involved the placement of solvent molecules using the program *Coot* (Emsley & Cowtan, 2004). Structure quality was assessed using *PROCHECK* (Laskowski *et al.*, 1993) and the structure-validation tools of *Coot*, which showed that 99.6% of the residues were in favourable regions and 0.4% were in disallowed regions; the offending residue was Tyr107, as has been previously observed (Dobson *et al.*, 2004, 2005). The r.m.s.d. for the subunits (all atoms) in the asymmetric unit was 0.57 Å, as calculated by *Coot* (Emsley & Cowtan, 2004). Data-collection and model-refinement statistics are summarized in Table 1.

2.4. Kinetic analysis

The catalytic rate of oxaloacetate decarboxylation by DHDPS was measured using a coupled assay with lactate dehydrogenase to detect pyruvate production. Briefly, oxaloacetate (final concentration 1 m*M*) was added to a cuvette pre-equilibrated to 303 K containing 0–1.6 µ*M* DHDPS, lactate dehydrogenase (>13 U) and 0.2 m*M* NADH in 100 m*M* sodium phosphate buffer pH 7.6. The rate of reaction was measured by observing the decline in absorbance of the NADH peak at 340 nm.

3. Results and discussion

The structure of DHDPS cocrystallized with oxaloacetate refined well, giving final refinement characteristics of R_{cryst} = 0.188 and R_{free} = 0.245, which were similar to those previously reported for the structure of native *E. coli* DHDPS (Dobson *et al.*, 2005). The cocrystallized structure has only one residue, Tyr107, lying in a disallowed region of the Ramachandran plot, as also observed in other DHDPS structures (Dobson *et al.*, 2004, 2005). This residue is part of the catalytic triad and is the central residue of a γ-turn located on a loop that projects from one subunit across the tight-dimer interface into the active site of another subunit (Blickling *et al.*, 1997; Dobson *et al.*, 2004, 2005; Mirwaldt *et al.*, 1995). There are two protein molecules in the asymmetric unit of the cocrystallized structure and each polypeptide molecule contained a pyruvate-bound active-site lysine (Lys161). The biologically relevant structure is a homo-tetramer, which is generated by crystallographic symmetry. In the final structure the pyruvate-bound adduct has been modelled as a Schiff base, although the structure refines equally well if the adduct is modelled as an enamine. The density is very well defined at the two active sites, with final refined B values in the range 18–24 Å^2, values that are very similar to those of the residues interacting with the pyruvate. Although the resolution of the structure is insufficient to distinguish reliably between the possible imine and enamine tautomers of the lysine adduct, there is no evidence from either subunit to suggest that the stereochemical restraints used were inappropriate. Importantly, in neither active site is there any density corresponding to the presence of the β-carboxylate moiety of oxaloacetate (Fig. 2).

[1] Supplementary material has been deposited in the IUCr electronic archive (Reference: SW5026).

Table 2
Hydrogen-bond lengths (Å) averaged between both active sites.

	Native	Native + pyruvate
Thr44 OH···Tyr133 OH	2.65	2.76
Thr44 OH···Tyr107b OH	2.64	2.69
Pyr CO1···Thr45 OH		2.75
Pyr CO1···Thr45 NH		2.94
Pyr CO2···Thr44 NH		2.84

Comparison of the structures of native DHDPS (PDB code 1yxc; Dobson *et al.*, 2005) and of DHDPS cocrystallized with oxaloacetate reveals a remarkable degree of similarity when the structures are overlaid (the r.m.s.d. fit based on C^{α} atoms for complete dimers is 0.24 Å and is 0.15 Å if the N-terminal methionine is excluded). In particular, there are no significant amino-acid movements in the active site, although a chloride ion that is found in the native structure hydrogen bonded to the ammonium N atom of Lys161 has been displaced to accommodate the pyruvate moiety (Fig. 3). Transfer of the proton from the lysine ammonium group to the pyruvate carboxylate group would generate an amine nucleophile for attack on the pyruvate carbonyl group. The carboxylic acid (or carboxylate) group of the pyruvate adduct forms hydrogen bonds to both the side-chain hydroxyl of Thr44 and the amide N atoms of Thr44 and Thr45. The orientation of the side chain of Asn248 cannot be unequivocally assigned; however, the orientation modelled, in which the $-NH_2$ moiety hydrogen bonds to Thr45 OG1, is consistent with the carboxylate of the lysine-bound pyruvate being either deprotonated or protonated *cis* to the imine N atom (see supplementary material). The latter arrangement sets up the Schiff base for tautomerization to the enamine species. The hydrogen-bonding network around the active site can only satisfy the alternate orientation of Asn248 if pyruvate is protonated *trans* to the imine N atom. For Asn248, this arrangement would be expected to lead to a high *B* value for OD1 and a low *B* value for ND2 relative to neighbouring atoms, as well as being stereochemically unfavourable for tautomerization of the pyruvate imine. Asn248 is well conserved (>70% among Swiss-Prot sequences annotated as DHDPS; data not shown) and is almost exclusively replaced by either a glycine or a serine when it is absent, in which case the contribution of Asn248 to the hydrogen-bonding environment may be played by an alternative residue or water molecule(s).

The catalytic triad of hydrogen-bonded residues that has been previously identified as being critical to activity is essentially undisturbed (Table 2; Dobson *et al.*, 2004). In the previously published (but low resolution and not deposited) pyruvate-bound structure (Blickling *et al.*, 1997) it was reported that the pyruvate carboxylate is oriented toward Tyr133, but in 3du0 the pyruvate lies approximately parallel to Tyr133, with the tyrosine hydroxyl group sitting near (3.58 Å) the imine C atom of the adduct (Fig. 3). This residue is thus well positioned to assist in initial formation of the Schiff base (Dobson *et al.*, 2004). Again in contrast to the report of Blickling *et al.* (1997), in which they describe a movement of Thr44 and Thr45 towards the pyruvate compared with the native structure, we do not observe any significant motion of any residues in the active site (Fig. 3,

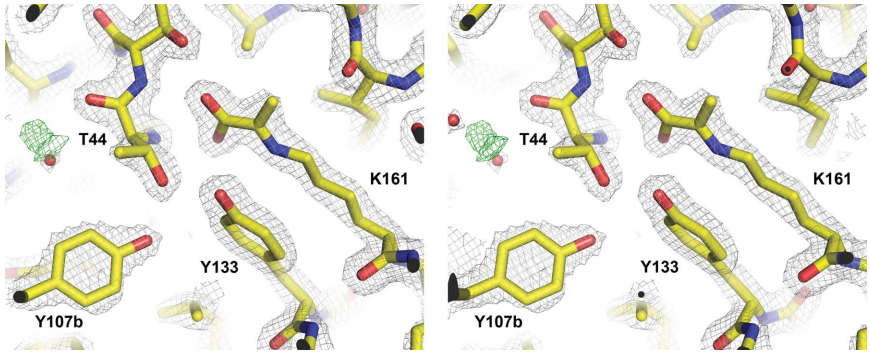

Figure 2
Stereoview of the active site of the refined structure showing pyruvate bound to the active-site lysine *via* an imine bond. $2F_o - F_c$ density (grey) is contoured at 2.0σ; $F_o - F_c$ density is contoured at 3.0σ (green) and -3.0σ (red). This figure was generated using *PyMOL* (DeLano, 2002).

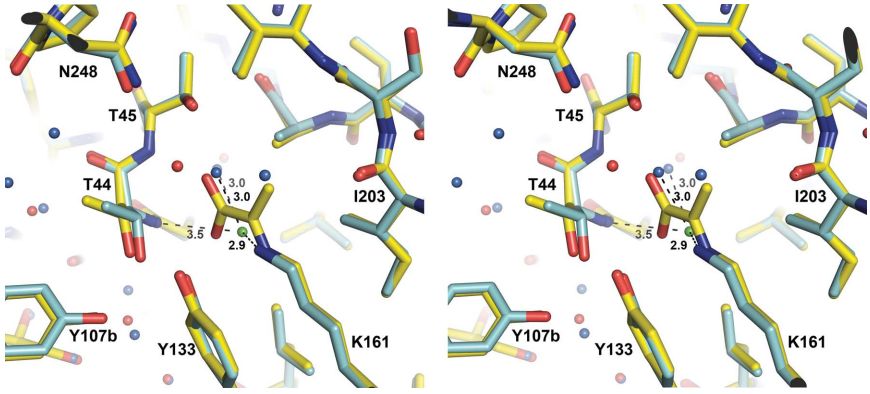

Figure 3
Stereoview of an overlay of the active site for the native (cyan, with blue waters) and pyruvate-bound (gold, with red waters) forms of *E. coli* DHDPS chain *A*. A chloride ion (green sphere) is present in the native structure and forms hydrogen bonds to the protein and two water molecules as indicated by the dashed lines (the lengths of each bond are given in Å). This figure was generated using *PyMOL* (DeLano, 2002).

Table 2). The pyruvate methyl group points out from the active site, being ideally positioned for the enamine tautomer to attack an incoming molecule of (*S*)-ASA, and is just 3.4 Å away from the carbonyl of Ile203, which has been proposed to play a role in imine/enamine tautomerization (Dobson *et al.*, 2008).

To eliminate the possibility that DHDPS is able to catalyse the decarboxylation of oxaloacetate as an explanation for the observed pyruvate adduct, we examined the rate of production of pyruvate (using lactate dehydrogenase) in the presence of differing quantities of DHDPS. The rate of pyruvate production was independent of DHDPS concentration, indicating that the decarboxylation of oxaloacetate was occurring by an enzyme-independent mechanism. It is known that oxaloacetate is able to decarboxylate spontaneously to pyruvate (Tsai, 1967) and that the reaction is catalysed by polyvalent cations (Speck, 1949), the presence of which as low-level contaminants in the protein preparation cannot be excluded. The occurrence of slow oxaloacetate decarboxylation during crystal growth would have provided pyruvate, which was then able to bind in the active site of DHDPS to give the observed structure.

The structure presented here reveals that on binding its first substrate, pyruvate, DHDPS does not undergo any structural rearrangements. The lysine-bound pyruvate is ideally oriented for the next step in the catalytic cycle in which as an enamine tautomer it attacks the terminal aldehyde of (*S*)-ASA. The structure is thus consistent with, and provides support for, the proposed catalytic mechanism of Dobson *et al.* (2004).

SRAD is grateful for funding from the Foundation for Research Science and Technology. Further funding was provided by the Royal Society of New Zealand Marsden fund (contract UOC303). Funding for the protein X-ray diffraction facility was provided in part by The Allan Wilson Centre for Molecular Ecology and Evolution. The authors wish to acknowledge Jackie Healy (University of Canterbury, New Zealand) for unswerving technical assistance.

References

Blagova, E., Levdikov, V., Milioti, N., Fogg, M. J., Kalliomaa, A. K., Brannigan, J. A., Wilson, K. S. & Wilkinson, A. J. (2006). *Proteins*, **62**, 297–301.
Blickling, S., Beisel, H., Bozic, D., Knäblein, J., Laber, B. & Huber, R. (1998). *J. Mol. Biol.* **274**, 608–621.
Blickling, S., Renner, C., Laber, B., Pohlenz, H.-D., Holak, T. A. & Huber, R. (1997). *Biochemistry*, **36**, 24–33.
Boughton, B. A., Dobson, R. C. J., Gerrard, J. A. & Hutton, C. A. (2008). *Bioorg. Med. Chem. Lett.* **18**, 460–463.
Collaborative Computational Project, Number 4 (1994). *Acta Cryst.* D**50**, 760–763.
Coulter, C. V., Gerrard, J. A., Kraunsoe, J. A. E. & Pratt, A. J. (1999). *Pestic. Sci.* **55**, 887–895.
Cox, R. J., Sutherland, A. & Vederas, J. C. (2000). *Bioorg. Med. Chem.* **8**, 843–871.
Curien, G., Biou, V., Mas-Droux, C., Robert-Genthon, M., Ferrer, J.-L. & Dumas, R. (2008). *Plant Physiol. Biochem.* **46**, 325–339.
DeLano, W. L. (2002). *The PyMOL Molecular Graphics System.* http://www.pymol.org.
Dobson, R. C. J., Griffin, M. D. W., Devenish, S. R. A., Pearce, F. G., Hutton, C. A., Gerrard, J. A., Jameson, G. B. & Perugini, M. A. (2008). *Protein Sci.* doi:10.1110/ps.037440.108.
Dobson, R. C. J., Griffin, M. D. W., Jameson, G. B. & Gerrard, J. A. (2005). *Acta Cryst.* D**61**, 1116–1124.
Dobson, R. C. J., Valegård, K. & Gerrard, J. A. (2004). *J. Mol. Biol.* **338**, 329–339.
Emsley, P. & Cowtan, K. (2004). *Acta Cryst.* D**60**, 2126–2132.
Frizzi, A., Huang, S., Gilbertson, L. A., Armstrong, T. A., Luethy, M. H. & Malvar, T. M. (2008). *Plant Biotechnol. J.* **6**, 13–21.
Hutton, C. A., Southwood, T. J. & Turner, J. J. (2003). *Mini-Rev. Med. Chem.* **3**, 115–127.
Kefala, G., Evans, G. L., Griffin, M. D. W., Devenish, S. R. A., Pearce, F. G., Perugini, M. A., Gerrard, J. A., Weiss, M. S. & Dobson, R. C. J. (2008). *Biochem. J.* **411**, 351–360.
Kefala, G. & Weiss, M. S. (2006). *Acta Cryst.* F**62**, 1116–1119.
Laskowski, R. A., MacArthur, M. W., Moss, D. S. & Thornton, J. M. (1993). *J. Appl. Cryst.* **26**, 283–291.
Miflin, B. J., Napier, J. & Shewry, P. R. (1999). *Nature Biotechnol.* **17**, 13–14.
Mirwaldt, C., Korndörfer, I. & Huber, R. (1995). *J. Mol. Biol.* **246**, 227–239.
Mitsakos, V., Dobson, R. C. J., Pearce, F. G., Devenish, S. R., Evans, G. L., Burgess, B. R., Perugini, M. A., Gerrard, J. A. & Hutton, C. A. (2008). *Bioorg. Med. Chem. Lett.* **18**, 842–844.
Pearce, F. G., Perugini, M. A., McKerchar, H. J. & Gerrard, J. A. (2006). *Biochem. J.* **400**, 359–366.
Pflugrath, J. W. (1999). *Acta Cryst.* D**55**, 1718–1725.
Speck, J. F. (1949). *J. Biol. Chem.* **178**, 315–324.
Tsai, C. S. (1967). *Can. J. Chem.* **45**, 873–880.
Vagin, A. A., Steiner, R. A., Lebedev, A. A., Potterton, L., McNicholas, S., Long, F. & Murshudov, G. N. (2004). *Acta Cryst.* D**60**, 2184–2195.
Vagin, A. & Teplyakov, A. (1997). *J. Appl. Cryst.* **30**, 1022–1025.